PHYSICAL REVIEW B VOLUME 43, NUMBER 14 15 MAY 1991-I

Temperature and doping-concentration dependence of the oscillatory properties of the photoreflectance spectra from GaAs grown by molecular-beam epitaxy

C. R. Lu, J. R. Anderson, D. R. Stone, W. T. Beard, and R. A. Wilson
Joint Program on Advanced Electronic Materials, University of Maryland, College Park, Maryland 20742 and Laboratory for Physical Science, College Park, Maryland 20740

T. F. Kuech and S. L. Wright
IBM Thomas J. Watson Research Center, Yorktown Heights, New York 10598
(Received 8 June 1990; revised manuscript received 14 January 1991)

The temperature and doping-concentration dependence of the oscillatory properties in the photoreflectance (PR) spectra of GaAs grown by molecular-beam epitaxy has been studied in detail. The peak separation of the oscillatory part of the PR spectrum is related to the internal electric field in the sample. Both the peak spacing of the oscillations and the internal electric field increase with increasing temperature and doping density. A PR spectrum with two kinds of oscillations from two interfaces across different doping profiles was also observed. Our study of oscillatory properties not only verified the electromodulation character of the PR experiment but also extracted the temperature dependence of the surface Fermi level.

I. INTRODUCTION

Recently photoreflectance (PR) has become one of the most popular among the modulated spectroscopy methods because no electrical contacts are required and it is a nondestructive technique.[1-3] However, the PR spectrum is more complicated than the external-field type of modulated optical spectrum, since in PR spectroscopy the electric field is provided by the space-charge distribution near the surface. The modulation is provided by a chopped pumping laser beam. The pumping photons generate free electron-hole pairs which tend to neutralize the space charge and thus flatten the band bending near the interface between different materials or between regions with different doping concentrations.

In addition to optical transition energies, information about the internal field near interfaces may be obtained from the oscillations in the PR spectrum.[4,5] Therefore, PR experiments may be used to study the temperature and doping-level variations of the internal electric fields in the semiconducting material. Nahory and Shay pioneered this type of study and showed that photoreflectance has the potential for the study of surface properties. Using different doping levels, they concluded from the PR spectra at 77 and 294 K that the PR effects originated primarily from the photomodulation of the surface field.[6,7] The increase of the spacing between the oscillation peaks in the PR spectra with increasing temperature and doping density may be explained by a simple Schottky-barrier model.

In the present work we applied the PR experiment to study the surface and internal electric-field variations in molecular-beam-epitaxy- (MBE-) grown GaAs layers versus temperature and doping densities. We have studied the PR spectra from the GaAs surface and the PR spectra from two types of doping profiles. The temperature ranged from 4.2 K to room temperature. The space-charge distribution, the band bending, and the internal electric field near the GaAs surface and the interfaces in the two types of doping profiles studied are illustrated schematically in Fig. 1. At the vacuum-GaAs interface there are surface states. Here we assume that these states take up carriers leaving a depleted region in the GaAs and an electric field whose modulation is responsible for the PR signal. Across the interface between the MBE-grown, *n*-type thin film and the undoped substrate, electrons will diffuse from the *n*-type region to the substrate and will induce an internal electric field which can also be modulated to generate the PR signal. The typical PR spectra of GaAs crystals, the line-shape variations versus temperature, and the dependence of the spectra on doping concentration are summarized in the next section. The information about the band bending extracted from the oscillation spacings is discussed in Sec. III. In Sec. IV we present the conclusions of our PR study.

II. EXPERIMENTAL RESULTS

Our experiments were performed with a standard PR setup using a He-Ne laser as the source of pumping photons as described in Ref. 1. The pumping and the probing beams were chopped at different frequencies, 214 and 352 Hz, respectively. The change of the reflectivity signal due to modulation was measured by a lock-in amplifier in phase with the sum frequency of the choppers. Using the double-chopping method, we were able to avoid the scattered laser light and reduce other background noise.[3]

Typical PR spectra from a 7×10^{15} cm^{-3} Si-doped GaAs surface at three different temperatures are shown in Fig. 2. The oscillating part of the spectrum above the

 ©1991 The American Physical Society

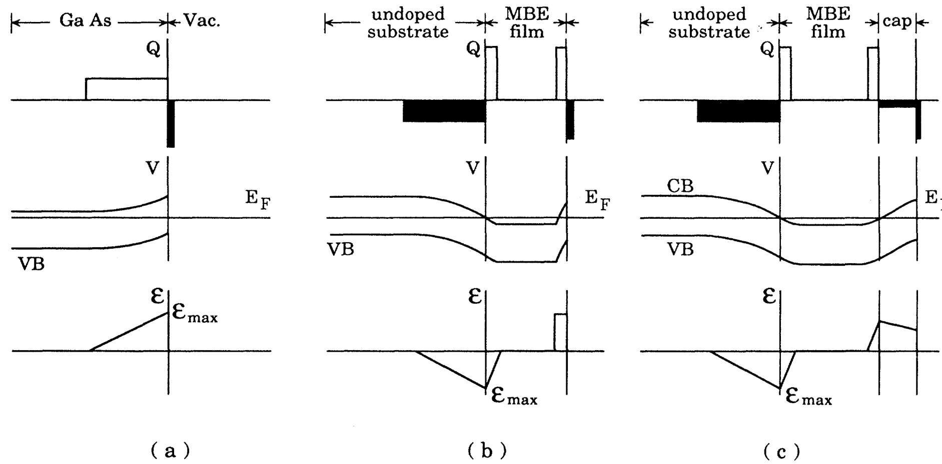

FIG. 1. Space-charge distribution Q, band-bending potential V, and internal electric field $\mathcal{E}$ are shown schematically for (a) GaAs surface, (b) the interface between a heavily doped thin film and an undoped substrate, and (c) the interface between a heavily doped thin film and an undoped substrate and the interface between a heavily doped thin film and an undoped cap. The open (solid) rectangular regions represent positive (negative) charges.

band gap is similar to Franz-Keldysh (FK) oscillations observed in electromodulated spectroscopy.[4,5] From Fig. 2 we see that the spacings of the oscillation peaks become larger when the temperature T increases. The PR spectra for different doping concentrations at a fixed temperature, 80 K, are shown in Fig. 3; the separation between oscillation peaks increases with doping concentration. This spreading of the spectra, shown in Figs. 2 and 3, indicates that the internal modulation field is increased with increasing temperature and doping concentration. Since the internal electric field in the semiconductor crystal is induced by the built-in potential across the space-charge region, the temperature dependence of this built-in potential across the interface may be obtained from the temperature dependence of the oscillation-peak spacings. The detailed relation will be discussed in Sec. III.

With increasing doping concentration the PR spectra start to lose the characteristics of a modulated reflectance line shape and become weaker and broader as shown in Fig. 4. At very high doping concentrations, $N_D > 10^{18}$ cm^{-3}, there is no detectable PR signal. The disappearance of the PR spectra may be due to the spatial fluctuations of the depletion depth caused by the random distribution of donors. If the sample is doped close to the three-halves power of the surface density of states, the depletion width will be approximately the average donor separation. Since the donors are randomly distributed, the uncertainty in the depletion width will be comparable to the width, and therefore a well-defined space-charge region with internal electric field will not exist. In this case, the PR experiment records the averaged information over a range of different modulation fields, the spectrum becomes broadened, and it loses its oscillatory character. Since the density of surface states varies from

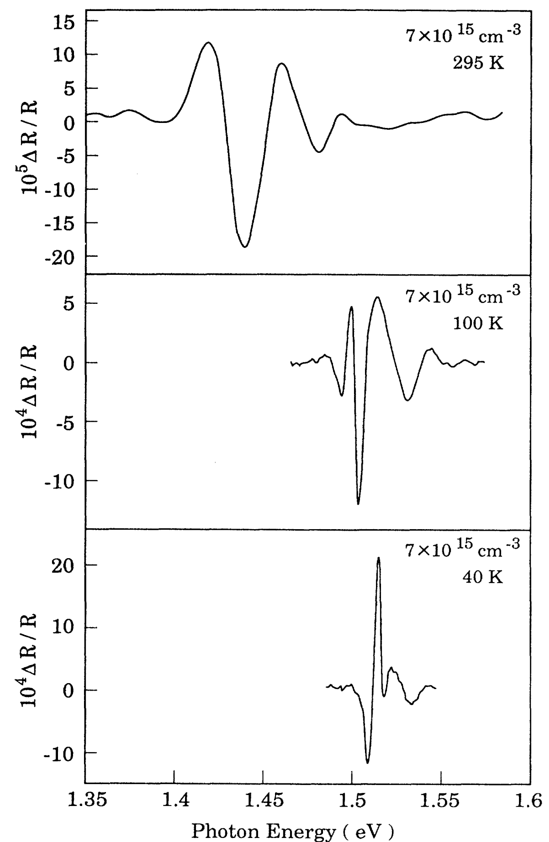

FIG. 2. PR spectra of 7×10^{15} cm^{-3} Si-doped GaAs at three different temperatures. Notice the peak-to-valley separations ΔE of the oscillations decrease with decreasing temperature.

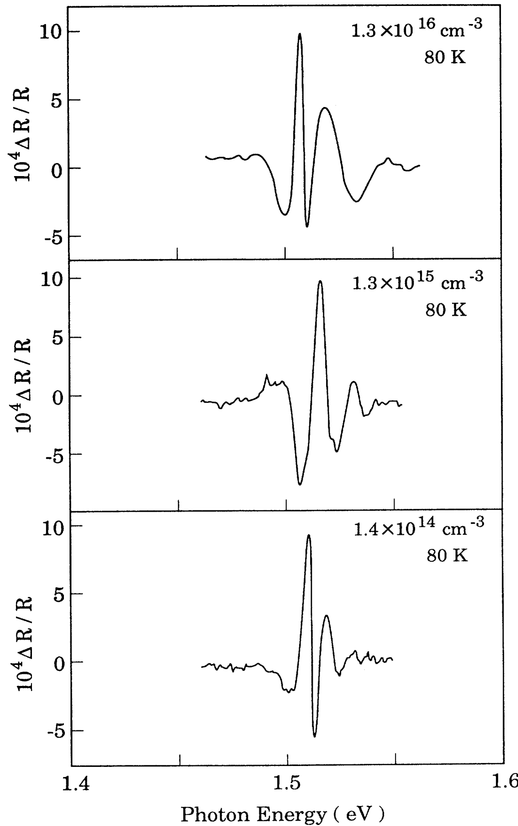

FIG. 3. PR spectra from the GaAs surfaces with three different doping concentrations. Notice the peak separations of the oscillations decrease with decreasing doping concentration.

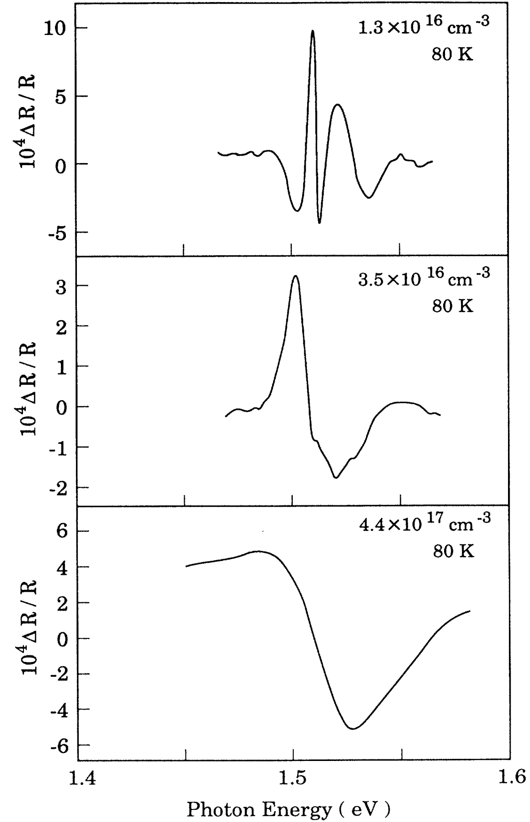

FIG. 4. PR spectra from surfaces of different highly doped GaAs samples. The PR spectra become broad and weak at high doping concentrations.

about 10^{11} to 10^{12} cm^{-2}, depending upon the surface quality, the three-halves power of the surface-state density varies from 3×10^{16} to 10^{18} cm^{-3}. We see from Fig. 4 that above 3×10^{16} cm^{-3} the PR spectrum already has become blurred and has lost its PR signature.

Although there is no PR signal observable from thick highly doped samples, it is possible to see the PR signal from thin highly doped samples. This is because the samples are so thin that photons are able to reach the interface between the undoped substrate and the heavily doped MBE layer. The band bending across this interface, as shown in Fig. 1(b), provides the modulation field needed for PR, and a PR signal originates from the back interface of the sample.

We studied two samples of this type of MBE thin film. One was a 0.3-μm-thick, 1.2×10^{19} cm^{-3} Sn-doped GaAs sample grown on an undoped substrate. The space-charge distribution, band bending, and electric field are shown schematically in Fig. 1(b). The other thin-film sample with thickness about 0.5 μm was a 5×10^{18} cm^{-3} Si-doped GaAs sample grown on an undoped substrate. There was a 0.05-μm undoped protection cap in front of the thin layer. There are two regions in the sample where the internal electric field is nonzero as shown in Fig. 1(c). In the cap region the electrons from the first layer of donors in the heavily doped region may be depleted to fill

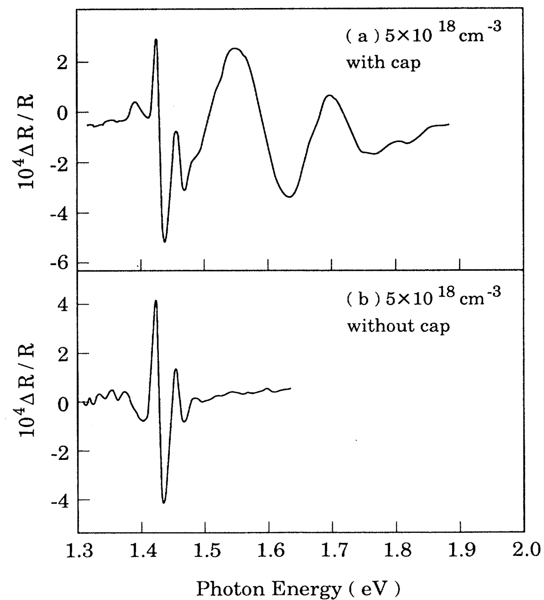

FIG. 5. PR spectra from the highly doped ($N_D-N_A=5\times10^{18}$ cm^{-3}) GaAs thin film with undoped protection cap. (a) Spectrum from both the front and back interfaces. (b) Spectrum from the back interface only. The cap was etched off.

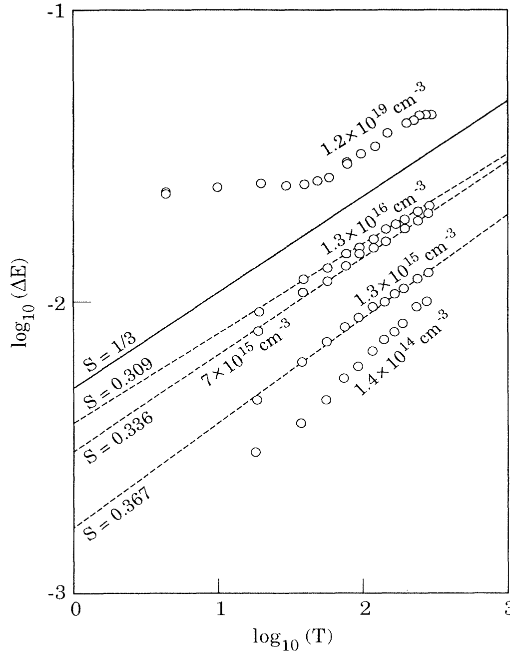

FIG. 6. The temperature variations of the oscillation spectra peak-to-valley spacings have been plotted on a log-log scale. The solid line in the figure, offset arbitrarily for ease of comparison, has a slope of $\frac{1}{3}$. The dashed lines with slopes S are least-squares fit to the data points.

up the surface states. A capacitorlike region will form between the positively charged depletion layer and the negatively charged surface and a large and slowly varying electric field will build up in this cap region. In this case the spatial fluctuations of the depletion depth will be small compared to the thickness of the capacitor region and the PR spectra will have large oscillatory peak spacings as shown in Fig. 5(a). On the back interface between the MBE layer and the undoped substrate, the space-charge region may extend farther into the undoped region and therefore the electric field will be smaller. The PR spectra will depend primarily on the electric field in the undoped region and consequently will have a small oscillation spacing. The PR spectrum with the cap etched off is shown in Fig. 5(b). It is clear that the portion of the spectrum in Fig. 5(a) with the large oscillation period is absent when the cap is removed.

The log of peak separations ΔE versus $\log(T)$ from four GaAs surfaces with different doping densities and from the back interface of the 1.2×10^{19} cm^{-3} Sn-doped sample are presented in Fig. 6. We see that ΔE is approximately proportional to $T^{1/3}$.

III. ANALYSIS

A. Qualitative interpretation

In the PR spectra, the signature of strength of the electric field is carried in the oscillations which are observed at energies greater than the gap energy. It is well known that both the one-electron band-to-band transition theory[4,5] and the excitonic transition theory[8–10] lead to an oscillatory electromodulated optical response above the band gap. A sharp exciton feature near the fundamental gap is predicted by the exciton theory. The PR spectrum near the fundamental gap is complicated and due to many different mechanisms.[6–14] Although the exciton effect has a strong influence in this region, a detailed analysis of this portion of the PR spectrum must be much more elaborate, and such an analysis is in progress. The oscillations above the fundamental gap, however, are due mainly to the electromodulation effect. In most calculations of the one-electron theory and the exciton theory, the photon energy $\hbar\omega$ may be replaced by a dimensionless energy η to deduce a general electromodulated spectrum and the line shape in terms of η is independent of the magnitude of the modulation field.[4,5,8–10] The dimensionless energy η is defined as $\eta=(\hbar\omega-E_g)/\hbar\Omega$, where

$$\hbar\Omega=\hbar\left[\frac{e^2\mathcal{E}^2\hbar^2}{8\mu}\right]^{1/3} . \tag{1}$$

E_g is the energy gap, μ is the reduced mass along the electric-field direction, $\mathcal{E}$ is the modulation electric field, e is the charge of the electron, and $\hbar$ is Planck's constant divided by 2π. To compare with an experimental spectrum, one needs to convert the theoretical spectrum from η units to the photon energy $\hbar\omega$ by multiplying $\hbar\Omega$ by η. Thus, the oscillation peak spacings in the large field-modulated spectrum will be larger than those in the small field-modulated spectrum. It is important to notice that both the one-electron theory and the exciton theory predict oscillatory features above the fundamental gap, but the oscillation amplitudes and the peak positions are different in the spectra deduced from two theories. On the other hand, the oscillation peak-to-valley spacings, ΔE, in the spectra with different modulation fields from the same sample will be proportional to the electro-optical energy $\hbar\Omega$, and

$$\Delta E=(\Delta\eta)\hbar\Omega ,$$

where $\Delta\eta$ is the oscillation peak-to-valley spacing in the theoretical spectrum in terms of the dimensionless unit η. From Eq. (1) we find that

$$\Delta E\propto\hbar\Omega\propto\mathcal{E}^{2/3} . \tag{2}$$

The internal electric field in the depletion region may be evaluated by integrating the Poisson equation. This electric field will have a maximum ε_{max} at the surface, given by

$$\mathcal{E}_{\text{max}}=\left[\frac{2eN_DV_{\text{bi}}}{\varepsilon_0}\right]^{1/2} . \tag{3}$$

Here N_D is the donor concentration and the band bending, $V_{\text{bi}}=(E_{\text{FB}}-E_{\text{FS}})$, is the built-in potential, which is equal to the difference between the Fermi level in the bulk (E_{FB}) and the Fermi level at the surface (E_{FS}). From Eqs. (2) and (3), it is easy to see that ΔE should de-

crease with decreasing doping concentration as shown in Fig. 6.

We now proceed to estimate the size of the band bending V_{bi}. The carrier concentration n may be described by the quasi-Fermi energy E_{FB} as

$$n = n_i \exp[(E_{FB} - E_i)/kT] , \quad (4)$$

where E_i is the intrinsic Fermi energy. For an n-type semiconductor with shallow donors, $n \approx N_D$, and the quasi-Fermi energy can be expressed as

$$E_{FB} = E_i + kT[\ln(N_D) - \ln(n_i)] , \quad (5)$$

where n_i is the intrinsic carrier density.

Since the surface Fermi energy of GaAs is pinned at midgap E_i, the band bending becomes proportional to the temperature when $N_D \gg n_i$ and the surface electric field $\mathcal{E}_{max}$ becomes proportional to the square root of the temperature. Therefore, the oscillation spacing ΔE will be proportional to the $\frac{1}{3}$ power of the temperature. The slopes of $\log_{10}(\Delta E)$ versus $\log_{10}(T)$ in Fig. 6 were very close to $\frac{1}{3}$ except for the lowest-doped and the heavily doped samples. In the lowest-doped sample, the internal electric field induced by the depleted donors is small. Therefore ΔE is also small and thermal broadening may dominate. Consequently, the broadening of the spectra, including only the electric-field effect, will underestimate ΔE at high temperatures. In addition, there are some background deep-level defects or donors whose density might be comparable with the small doping concentration. In this case, as the temperature decreases, the electrons from deep levels freeze out quickly and the relative space-charge density decreases faster with temperature than expected from normal donors and so does the internal electric field.

As to the heavily doped sample, the substrate Fermi energy is not necessarily pinned at midgap and the Fermi energy in the heavily doped layer is degenerate with the conduction band. The simplified quasi-Fermi-level description of the band bending is not applicable.

B. Calculation of Fermi energies

In this section we calculate the Fermi energy in different regions of the sample in a more rigorous way to obtain band bending information. For a nondegenerate bulk crystal, the calculation starts with the charge neutrality equation, which may be written as

$$N_A \frac{1}{1+4\exp[(E_A - E_{FB})/kT]} + N_c \exp[-(E_c - E_{FB})/kT] = N_D \frac{1}{1+2\exp[(E_{FB} - E_D)/kT]} + N_v \exp[(E_v - E_{FB})/kT] , \quad (6)$$

where N_c and N_v are effective densities of states in the conduction band and valence band, respectively. In Eq. (6) N_D and N_A are doping densities of donors and acceptors and E_D and E_A are donor and acceptor levels. For an n-type semiconductor, the unintentionally doped acceptors ($N_A \ll N_D$) may be ignored for simplicity. For a given set of N_c, N_D, N_v, E_c, E_D, E_v, and T the Fermi energy can be uniquely determined from Eq. (6). Figure 7 illustrates the calculated Fermi energies versus temperature for GaAs with doping concentrations from 10^{12} to 10^{17} cm^{-3}. If the surface Fermi energy is pinned at the midgap at all temperatures, it is clear from Fig. 7 that band bending will increase when the temperature decreases. Since this is contrary to the result observed, we suggest that the Fermi energy at the surface does not remain constant when the temperature changes.

There has been an intensive effort in recent years to characterize interfaces between metals and III-V compound semiconductors, with a strong emphasis placed on GaAs. It was established early on for GaAs that, despite a variety of interface structural properties and chemical interactions with metals, the surface Fermi level (E_{FS}) at room temperature is pinned within a small range near midgap, giving a barrier height nearly independent of the metal work function.[15] Models based on native defects,[16] interface chemistry,[17] effective work functions,[18] and metal-induced gap states[19] have been proposed to explain this behavior, but there remains considerable controversy about this issue. The morphology, chemistry, and atomic structure of metal-(III-V) interfaces are complex and diverse, and there is no consensus at this point on the mechanism(s) which dominate pinning during interface formation.

The temperature dependence of the surface Fermi-level pinning has not yet been well understood either theoretically or experimentally. Although almost all the experimental information related to the GaAs surface Fermi-

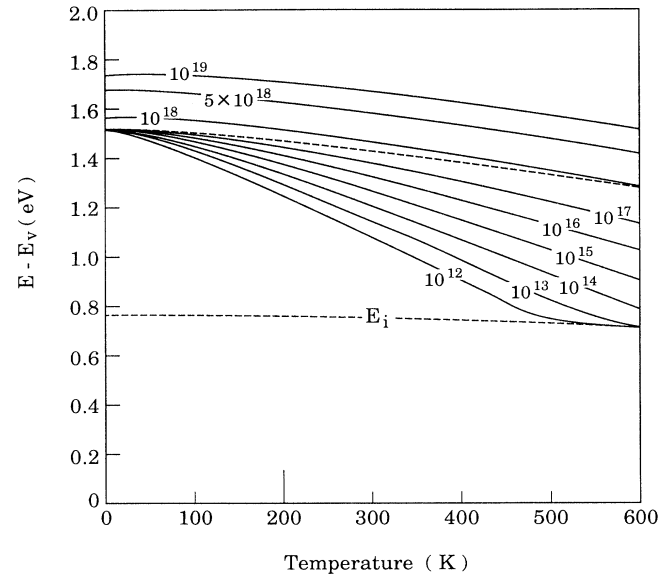

FIG. 7. Calculated temperature dependence of Fermi levels of bulk GaAs with different doping concentrations (solid lines). The upper dashed curve indicates the conduction-band edge and the lower dashed curve indicates the intrinsic Fermi level.

level pinning was obtained at room temperature, a few low-temperature studies were performed near liquid-nitrogen temperature;[20–23] these experimental results indicate that the surface Fermi energy approaches the bulk Fermi level at low temperatures. Therefore, for our calculation, we assume that for *n*-type GaAs the surface Fermi energy increases linearly from midgap at room temperature to the zero-temperature pinning position near the conduction band.

The assumed temperature variation of the surface Fermi energy used in the calculation for the 1.3×10^{16} cm^{-3} GaAs-oxide interface is shown in Fig. 8 by a straight line labeled E_{FS}. This temperature variation combined with the bulk Fermi energy E_{FB}, calculated from Eq. (6), was used to calculate the difference between the bulk and the surface Fermi level and thus to obtain the built-in potential. The temperature variations of the surface and the bulk Fermi energies are given in Fig. 8(a). We see that the built-in potential, $(E_{FB}-E_{FS})$, decreases approximately linearly with decreasing temperature. To compare with experiment, we used our calculated built-in potential to obtain the electric field from Eq. (3) and the electro-optical energy $\hbar\Omega$ from Eq. (1). The temperature variation of Ω is observed in the PR spectra by measuring the oscillation peak spacing, which is proportional to Ω, Eq. (2). Therefore, we normalized the observed peak-to-valley spacing, ΔE, of the oscillation spectrum as $\Delta E(T)/\Delta E(T_0)=\Omega(T)/\Omega(T_0)$, with T_0 chosen as 200 K. A comparison of the normalized Ω from calculations with the experimental data is shown in Fig. 8(b). Since the calculations agree quite well with the experimental observations, our assumed temperature dependence for the surface Fermi level is plausible.

For the highly doped sample, the Fermi energy is degenerate with the conduction band. That is, the electron gas behaves like an ideal gas in a positive-charge background of ionized donors. However, since the size of the donor wave function exceeds the average separation between impurities, quantum-mechanics averaging smears out the discrete charge of an individual impurity and the density of states will have an exponential tail into the forbidden gap (see Refs. 24 and 25). Therefore the Fermi-level position cannot be determined from the simple expression, Eq. (6). We have calculated the Fermi levels for heavily doped bulk crystals using expressions from Refs.

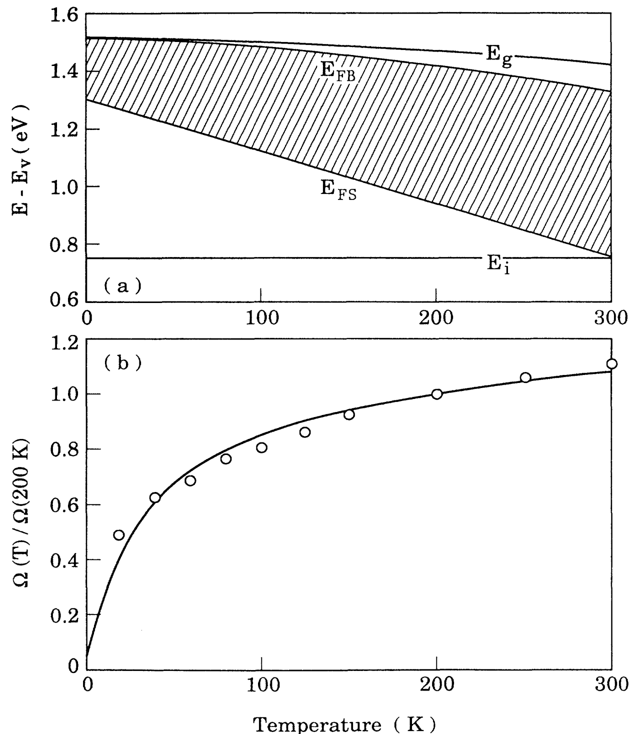

FIG. 8. The temperature variations of the surface and the bulk Fermi energies for the 1.3×10^{16} cm^{-3} Si-doped sample are given in (a) by the curves E_{FS} and E_{FB}, respectively. The observed temperature dependence of the electro-optical energy, Ω (circles), is compared with the calculated results (solid line) in (b). The calculation is based on the built-in potential, $E_{FB}-E_{FS}$, illustrated in the shaded area in (a), where E_g and E_i are energy gap and intrinsic Fermi level, respectively.

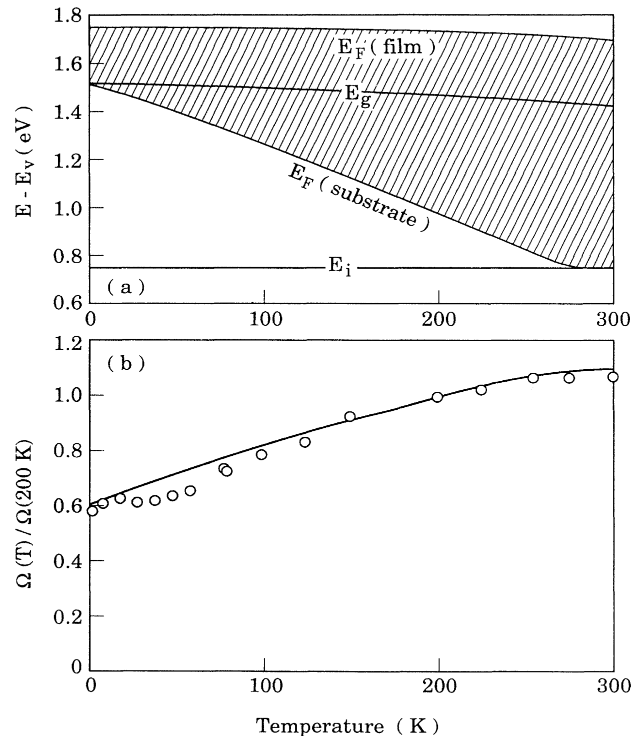

FIG. 9. The temperature variations of the epitaxial layer and the substrate Fermi energies for the 1.2×10^{19} cm^{-3} Sn-doped sample are given in (a) by the curves E_F (film) and E_F (substrate), respectively. The observed temperature dependence of the electro-optical energy, Ω (in circles), is compared with the calculated results (solid line) in (b). The calculation is based on the built-in potential illustrated in the shaded area in (a), where E_g and E_i are energy gap and intrinsic Fermi level, respectively.

24 and 25 and results are shown by the top three curves in Fig. 7.

The band bending may be obtained from the difference between the Fermi level in the undoped substrate and the Fermi energy in the heavily doped MBE thin layer. The temperature dependence of this band bending, i.e., the built-in potential, across an undoped substrate, $N_D \simeq 10^{14}$ cm^{-3}, and heavily doped, $N_D \simeq 1.2 \times 10^{19}$ cm^{-3}, MBE film is shown in Fig. 9(a). In this calculation, a small concentration of acceptors, $N_A \simeq 10^{14}$ cm^{-3} and $E_A \simeq 0.03$ eV, in the substrate was needed to fit with the observed electro-optical energy Ω in Fig. 9(b). These acceptors may be from carbon ($E \sim 0.026$ eV) or other impurities in the substrate.[26] Comparing Fig. 9 with Fig. 8, we see that the electro-optical energy does not approach zero in the heavily doped sample at low temperatures because the carriers do not become frozen out on the donors. We also note from Fig. 9 that, although the calculations agree well with the observations, there is some deviation in the low-temperature region. This deviation may be due to *DX* centers in the heavily doped samples. When the temperature is below about 50 K, electrons trapped on *DX* centers cannot overcome the thermal barrier of the *DX* center[27] and therefore the Fermi energy, evaluated on the assumption that the number of free electrons equals the number of donors, may not be correct. A detailed investigation of the properties of the *DX* centers in these heavily doped samples is in progress.

IV. CONCLUSIONS

In this study of photoreflectance, the oscillatory properties in the PR spectra were studied for GaAs surfaces and interfaces across the regions with different doping densities. The temperature dependence of the oscillation spacings in the PR spectra for different doping concentrations may be explained well by the temperature variations of the Fermi energies at the surface and in the bulk crystal. It should be possible to study the internal electric-field distribution in $Al_{1-x}Ga_xAs/GaAs$ heterostructures by examining similar oscillatory properties in the PR spectrum.

ACKNOWLEDGMENTS

We wish to thank Professor D. H. Drew, Dr. M. Gorska, Dr. R. Mani, and Dr. D. K. Gaskill for many helpful discussions and much valuable assistance. This work has been supported in part by the U.S. Defense Advanced Research Projects Agency and Army Research Office under Grant No. DAAG-29-85-K-0052.

[1] F. H. Pollak and O. J. Glembocki, Proc. SPIE **946**, 2 (1988).
[2] M. Cardona, Bull. Am. Phys. Soc. **34**, 660 (1989).
[3] C. R. Lu, J. R. Anderson, W. T. Beard, and R. A. Wilson, Superlatt. Microstruct. **8**, 155 (1990).
[4] N. Bottka, D. K. Gaskill, R. S. Sillmon, R. Henry, and R. Glosser, J. Electron. Mater. **17**, 161 (1988).
[5] D. Aspnes and N. Bottka in *Semiconductors and Semimetals,* edtied by R. K. Willardson and A. C. Beer (Academic, New York, 1972), Vol. 9.
[6] R. E. Nahory and J. L. Shay, Phys. Rev. Lett. **21**, 1569 (1968).
[7] J. L. Shay, Phys. Rev. B **2**, 803 (1970).
[8] H. I. Ralph, J. Phys. C **1**, 378 (1968).
[9] J. D. Dow and D. Redfield, Phys. Rev. B **1**, 3358 (1970).
[10] D. F. Blossey, Phys. Rev. B **2**, 3976 (1970); **3**, 1382 (1971).
[11] M. Sydor, J. Angelo, J. J. Wilson, W. C. Mitchel, and M. Y. Yen, Phys. Rev. B **40**, 8473 (1989).
[12] M. Cardona, K. L. Shaklee, and F. H. Pollak, Phys. Rev. **154**, 696 (1967).
[13] J. G. Gay and L. T. Klauder, Jr., Phys. Rev. **172**, 811 (1968).
[14] D. E. Aspnes and A. Frova, Phys. Rev. B **2**, 1037 (1970).
[15] W. E. Spicer, I. Lindau, P. E. Gregory, C. M. Garner, P. Pianetta, and P. W. Chye, J. Vac. Sci. Technol. **13**, 780 (1976).
[16] W. E. Spicer, P. W. Chye, P. R. Skeath, C. Y. Su, and I. Lindau, J. Vac. Sci. Technol. **16**, 1422 (1979).
[17] L. J. Brillson, Surf. Sci. Rep. **2**, 123 (1982).
[18] J. Freeouf and J. M. Woodall, Appl. Phys. Lett. **39**, 727 (1981).
[19] J. Tersoff, Phys. Rev. Lett. **52**, 465 (1984).
[20] K. Stiles, A. Kahn, D. G. Kilday, and G. Margaritondo, J. Vac. Sci. Technol. B **5**, 987 (1987).
[21] K. Stiles, D. Mao, and A. Kahn, J. Vac. Sci. Technol. B **6**, 1170 (1988).
[22] R. Cao, K. Miyano, T. Kendelewicz, K. K. Chin, I. Lindau, and W. E. Spicer, J. Vac. Sci. Technol. B **5**, 998 (1987).
[23] R. Cao, K. Miyno, T. Kendelewicz, I. Lindau, and W. E. Spicer, Surf. Sci. **206**, 413 (1988).
[24] E. O. Kane, Phys. Rev. **131**, 79 (1963).
[25] M. I. D'yakonov, A. L. Efros, and D. L. Mitchell, Phys. Rev. **180**, 813 (1969).
[26] S. M. Sze and J. C. Irvin, *Solid State Electron.* **11**, 599 (1968).
[27] T. N. Theis, P. M. Mooney, and S. L. Wright, Phys. Rev. Lett. **60**, 361 (1988).